CCS Chemistry

RESEARCH ARTICLE

Received: Apr. 29, 2022 | Accepted: June 8, 2022 | Published: June 30, 2022

Tuning Ice Nucleation by Mussel-Adhesive Inspired Polyelectrolytes: The Role of Hydrogen Bonding

Jing Chen[1,2*†], Yongkang Wang[2,3†], Benjamin Leibauer[2], Takakazu Seki[2], Konrad Meister[2,4], Yuki Nagata[2*] & Mischa Bonn[2*]

[1]*Department of Chemistry, School of Science, Tianjin University of Science & Technology, Tianjin 300457,* [2]*Max Planck Institute for Polymer Research, Mainz 55128,* [3]*School of Mechanical Engineering, Southeast University, Nanjing 211189,* [4]*School of Arts & Sciences, University of Alaska Southeast, Juneau, Alaska 99801*

**Corresponding authors: chenj2@mpip-mainz.mpg.de; nagata@mpip-mainz.mpg.de; bonn@mpip-mainz.mpg.de;* [†] J. Chen and Y. Wang contributed equally to this work.

Cite this: *CCS Chem*. **2022**, Just Published. DOI: 10.31635/ccschem.022.202202087

Heterogeneous ice nucleation (HIN) on foreign surfaces plays a crucial role across a wide range of environmental and biological processes, and control of HIN is highly desirable. Functionalizing surfaces to control HIN poses interesting scientific challenges and holds great potential for technological impact. Here, we combine the ice nucleation tuning capability of polyelectrolytes with mussel-inspired adhesives to obtain robust surface functionalization with HIN control. We tune ice nucleation by integrating strongly surface-binding catechol derivatives into three different polyelectrolytes via a facile and scalable strategy. Sum-frequency generation (SFG) spectroscopy reveals that the functionalized surface with the lowest ice nucleation temperature (−22.1 °C) exhibits the strongest hydrogen bonding interaction with water molecules. The coating exhibits long-term stability up to 30 days even under harsh conditions such as 5 M salt solution and can be deposited onto various substrates because of its strong adhesion on solid surfaces. Moreover, the precise ice nucleation temperature window can be tuned by controlling the grafting degree of the catechol derivatives. Our study provides a new strategy for tuning ice nucleation and provides a new perspective on understanding the mechanism of ice nucleation at the molecular level by interfacial molecular spectroscopy, which will help in the design and development of anti-ice-nucleation materials.

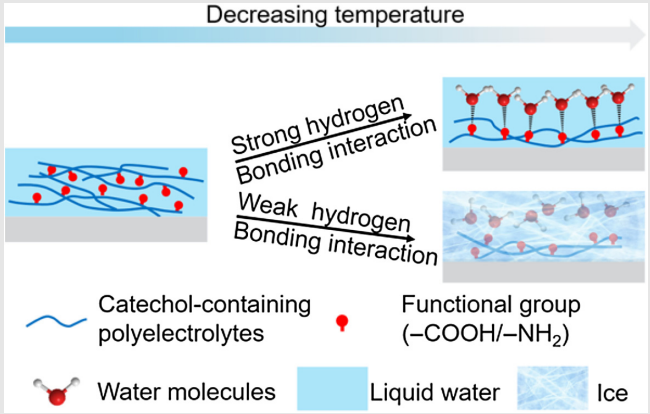

Keywords: **ice nucleation, polyelectrolyte, catechol, sum-frequency generation, hydrogen bonding**

Introduction

The undesired formation and accumulation of ice can lead to severe problems in our daily life, ranging from the accelerated deterioration of transmission lines and buildings to the damage of plants, causing economic and energy losses.[1-5] The icing of surfaces starts with ice nucleation, followed by growth and propagation[6] and adherence to and accumulation on the surface.[7,8] Tuning ice nucleation, controlling ice growth and propagation,

and reducing ice adhesion are three main strategies for confronting icing problems.[9,10] Water freezing at a solid surface is a process of ice nucleation and growth, in which nucleation plays a key role. It is assumed that nucleation occurring at the liquid–solid interface is dominated by heterogeneous nucleation at low supercooling temperatures.[11] Heterogeneous ice nucleation (HIN) often starts on foreign surfaces and is governed by surface-inherent properties such as interfacial free energy, interfacial geometry, and lattice match.[12] To control ice growth and propagation, hygroscopic materials and structural design are often employed to disturb ice bridging or weaken ice propagation.[13,14] If the ice nucleation and propagation cannot be effectively controlled, the ice will become thicker and denser on the surface. Reducing ice adhesion is the last line of defense against ice. There is a growing body of literature that focuses on the reduction of ice adhesion,[15–21] with a reduction of ice adhesion to below 10 kPa according to a recent study.[22] Such weak adhesion allows ice to be easily shed off from the surface by the action of wind or gravity. However, ice nucleation is the initial and rate-limiting step of the ice formation.[23] In this regard, special attention should be given to ice nucleation, especially for tuning HIN.

Antifreeze (glyco)proteins (AF(G)Ps) protect a variety of organisms inhabiting subzero environments by efficiently controlling ice growth, and thus have been employed to modify surfaces to control ice nucleation.[24–26] Inspired by AF(G)Ps, polypeptides have been designed and synthesized to suppress ice nucleation or retard recrystallization. Yang et al.[27] tethered supercharged polypeptides with different surface charges and charge densities onto a surface to regulate ice nucleation, and they attributed the change of ice nucleation temperature on that charged surface to the asymmetric polarization of interfacial water. By mimicking AFPs, Wang designed and engineered self-assembling peptides, which showed moderate inhibition of ice crystal growth and recrystallization owing to the alignment of threonine residues with their intervals matching the ice lattice.[28] To immobilize AF(G)Ps or polypeptides onto the surface, pre-functionalization of the substrate is required before it is coated, that is, a special functional group must first be bound on the surface of the substrate, thereby restricting the widespread application of AF(G)Ps due to the complex procedure.[29] Therefore, a universal, easily applicable coating that can be applied to various solid surfaces for tuning ice nucleation is highly desired.

Fortunately, nature has again provided us with a potential strategy to overcome these challenges. Recently, mussel proteins have attracted much attention because they can strongly stick to virtually any type of substrate with high binding strength via secreting *Mytilus edulis* foot protein.[30,31] Their extraordinary ability to stick to most inorganic and organic surfaces is traced to the high levels of catechol and amine functional groups in the mussel foot protein (mfp, see Figure 1a).[32–34] Hong et al.[35] indicated that both covalent and non-covalent interactions between the catechol derivatives and substrates are responsible for strong catechol adhesion. Consequently, this biomimetic concept offers a new avenue for constructing coatings for tuning ice nucleation.

Benefiting from the strong adhesive property of catechol derivatives and the diversity of functional groups of polyelectrolytes, we designed a series of catechol-containing polyelectrolytes (CPs). Three different CPs were prepared using an amidation reaction through a facile and green one-step procedure for tuning ice nucleation. Of these three, the surface coated by catechol-containing branched poly(ethylenimine) (bPEI-C) shows good ice nucleation suppression, and it can be applied to various surfaces due to the nonselective adhesion of catechol groups. The range of HIN temperature (T_H) could be enlarged after cross-linking by controlling the molar feed ratio between the catechol derivative and polyelectrolyte. Our analysis using surface-specific vibrational spectroscopy reveals that the interactions between functional groups of polyelectrolytes and interfacial water molecules play a key role in tuning ice nucleation for polyelectrolytes. The ice nucleation temperature decreases for stronger interactions between the functional groups of polyelectrolytes and water molecules. In addition, the bPEI-C coating maintains excellent stability under harsh conditions and can be prepared on a large scale, showing excellent application prospects.

Experimental Methods

Materials and instrumentation

All chemicals were obtained from commercial sources and used without further purification. The absorbance spectra of the prepared CPs were obtained using a Cary 60 UV–vis spectrophotometer (Agilent, Santa Clara, California, United States). Fourier transform infrared (FT-IR) spectra were recorded by the attenuated total reflection method with an FT-IR spectrometer (Tensor II, Bruker, Rosenheim, Germany). Proton nuclear magnetic resonance (^{1}H NMR) spectra were recorded at 300 MHz on a Bruker AVANCE III 300 NMR spectrometer. X-ray photoelectron spectroscopy (XPS) was performed on the Thermo Scientific ESCALab 250Xi (Thermos Scientific, Waltham, Massachusetts, United States) using 200 W monochromatic Al K_α radiation. The base pressure in the analysis chamber was approximately 3×10^{-9} mbar. The pass energy was 30 eV. The

Citation: *CCS Chem.* **2022**, Just Published. DOI: 10.31635/ccschem.022.202202087
Link to VoR: https://doi.org/10.31635/ccschem.022.202202087

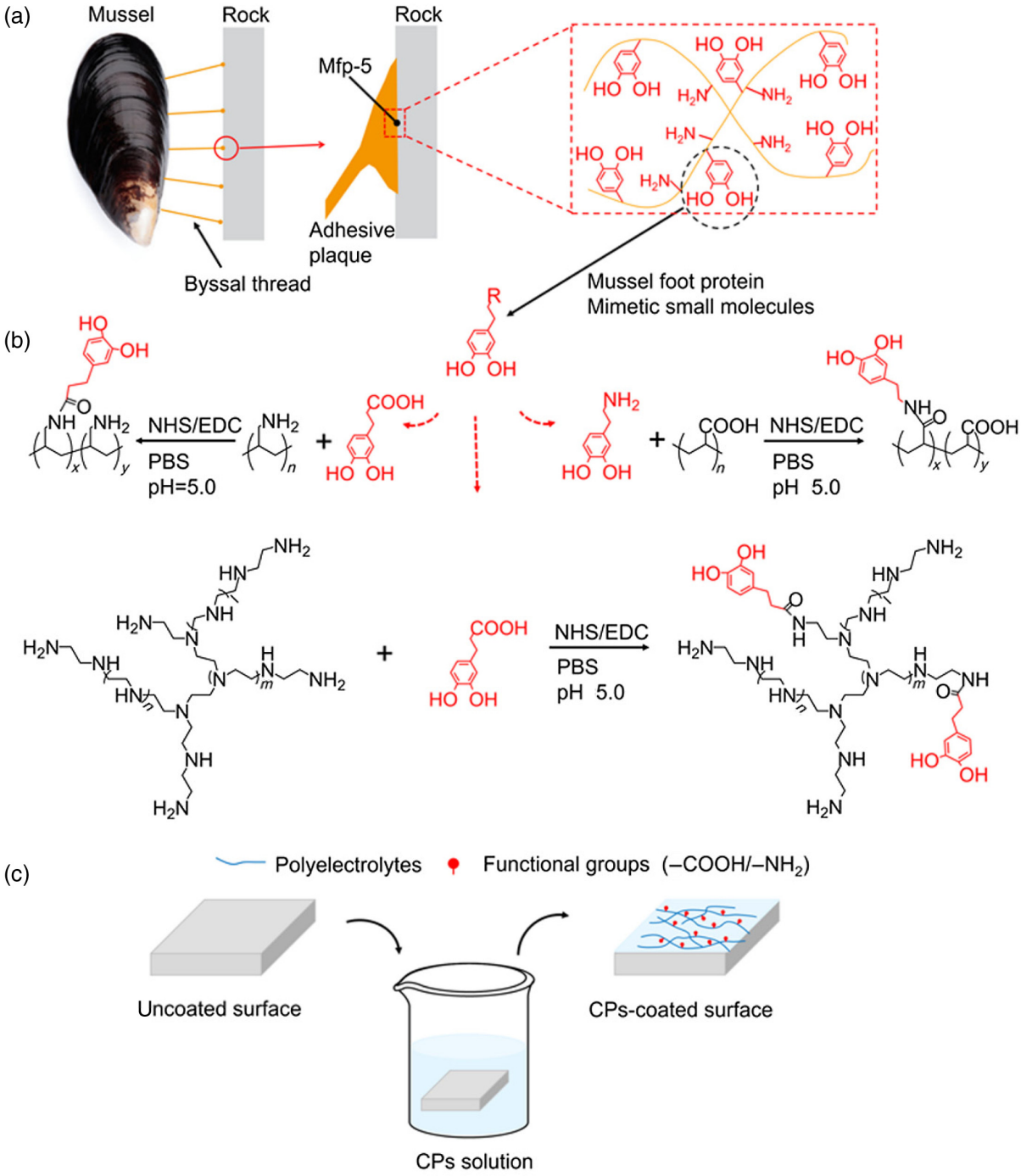

Figure 1 | *(a) Schematic of a mussel anchored by byssal threads and adhesive plaques to a rock and the interfacial location of mfp-5 with a simplified molecular representation of characteristic amine and catechol groups. (b) Synthesis of the CPs. DA and DOPA both contain catechol functional groups and were used as mfp-mimetic small molecules for grafting the polyelectrolytes onto solid surfaces. (c) Schematic representation of the process of the CP coating.*

static contact angle (CA) on the samples was measured at room temperature with a CA System (DataPhysics Instruments OCA35 goniometer, Dataphysics, Stuttgart, Germany). The average CA values were obtained by measuring at five different positions on the same sample. The morphologies of the solid substrates before and after coating by the CPs were obtained by atomic force microscopy (AFM) (NanoWizard 4, JPK Instruments, Berlin, Germany) in the tapping mode. Tapping mode etched silicon probes OTESPA with aluminum reflective coating on the

Citation: *CCS Chem.* **2022**, Just Published. DOI: 10.31635/ccschem.022.202202087
Link to VoR: https://doi.org/10.31635/ccschem.022.202202087

backside of the cantilever were used (cantilever resonance frequencies were approximately 300 kHz; a typical spring constant 26 N m^{-1}). The scan size was 2 μm × 2 μm with 512 × 512 pixels.

Synthesis of catechol-containing PAH, PAA, and bPEI

Synthesis of PAA-C

An aqueous solution of poly(acrylic acid) (PAA; 1.2 g of a 35 wt % solution) was diluted with 0.1 M phosphate-bufferred solution (PBS) (30 mL). Then 115.0 mg 1-Ethyl-3-(3-dimethyllaminopropyl)carbodiimide hydrochloride (EDC·HCl) and 69.1 mg N-Hydroxysuccinimide (NHS) was added to the above solution. Then, 113.8 mg dopamine (DA) hydrochloride was added. The reaction solution was adjusted to pH 5.0 with 1.0 M NaOH and HCl and stirred for 24 h under N_2 gas protection.

Synthesis of PAH-C and bPEI-C

3-(3,4-dihydroxyphenyl) propionic acid (DOPA; 109.3 mg) was dissolved in 0.1 M PBS (50 mL) followed by EDC·HCl (115.0 mg) and NHS (69.1 mg). The solution was stirred for 2 h. The poly(allylamine) (PAH; 1.7 g of a 20 wt % solution) or bPEI (360 mg) was dissolved in 0.1 M PBS (30 mL) and then added to the above solution, and the reaction solution was adjusted to pH 5.0 with 1.0 M NaOH and HCl and stirred for 24 h.

The resultant mixture was dialyzed by a regenerated cellulose membrane (molecular weight cut-off = 3500) in deionized water. The final conjugates were lyophilized.

The construction of coating on the solid substrates

The CPs were dissolved in deionized water at a concentration of 1 mg/mL. Then the pH was adjusted to 8.0 with 1M NaOH and HCl. The cleansed substrates were incubated in the above solution for 6 h. Then the solid substrates were removed, rinsed with ultrapure water, and dried under a stream of nitrogen gas.

Characterization

The ice nucleation temperatures and freezing delay time on CP-coated surfaces were performed by a homemade experimental apparatus with a microscope coupled with a high-speed camera and a cryostage, as described elsewhere.[27,36] Our $\mathrm{Im}\chi^{(2)}_{\mathrm{eff}}$ spectra were measured using Heterodyne-Sum Frequency Generation (HD-SFG) spectroscopy at ssp polarization combination, where ssp denotes s-polarized sum-frequency generation (SFG), s-polarized visible, and p-polarized IR beams. Further details about ice nucleation measurement and SFG measurement can be found in the Supporting Information.

Results and Discussion

Synthesis and characterization of CPs and CP-coated surfaces

Inspired by the strong adhesion due to the catechol and amine groups in mfps (Figure 1a), DA and DOPA were used as mfp-mimetic small molecules and were grafted to PAA, PAH, and bPEI, respectively (Supporting Information Figure S1). As seen in Figure 1b, three types of CPs were synthesized by the conjugation of catechol derivatives with polyelectrolytes via an amidation reaction between amino and carboxyl groups under mild synthetic conditions. The resulting catechol-grafted polymers were denoted as PAH-C, PAA-C, and bPEI-C. The successful introduction of the DA or DOPA into polyelectrolytes was evidenced by UV–vis spectroscopy, FT-IR, and ^{1}H-NMR analysis (see Supporting Information Figure S2).[37–39]

Figure 1c illustrates the fabrication procedure of the CP coating. First, CPs were dissolved in water, and cleaned silicon wafers were immersed in the solution. CP-coated surfaces were obtained after incubation for a few hours due to the strong adhesion of the catechol groups.[40] XPS was utilized to characterize the surface composition. A new peak of the N 1s on the PAA-C coated surface and intense N 1s peak on PAH-C- and bPEI-C-coated surfaces indicated that CPs were successfully deposited on the silicon wafer surface (Supporting Information Figure S3). AFM measurements shown in Supporting Information Figure S4 revealed a root mean square roughness of the CP-coated surfaces of less than 3 nm, exhibiting relatively homogeneous and smooth surfaces. After coating with the CPs, we found that the static contact angle on the PAA-C coated surface was lower than that of the PAH-C coated surface (Supporting Information Figure S5). But the bPEI-C coated surface had the lowest water contact angle, which indicates a better affinity between the amino groups and the water molecules due to the highly branched structure of bPEI.

Ice nucleation

The ice nucleation temperature was determined by measuring the freezing temperatures of condensed microdroplets on CP-modified surfaces in a homebuilt closed cell to avoid possible extraneous effects. We placed a macrodroplet of ultrapure water (Milli-Q, 18.2MΩ cm) at the edge of the sample surface in a closed chamber with a relative humidity of 100%. Then, many microdroplets appeared on the CP-modified surfaces via an evaporation–condensation process (Supporting Information Figure S6). Afterward, the nucleation temperature of the condensed microdroplets was recorded as the sample surface temperature was lowered. This evaporation–condensation method is widely used

Citation: *CCS Chem.* **2022**, Just Published. DOI: 10.31635/ccschem.022.202202087
Link to VoR: https://doi.org/10.31635/ccschem.022.202202087

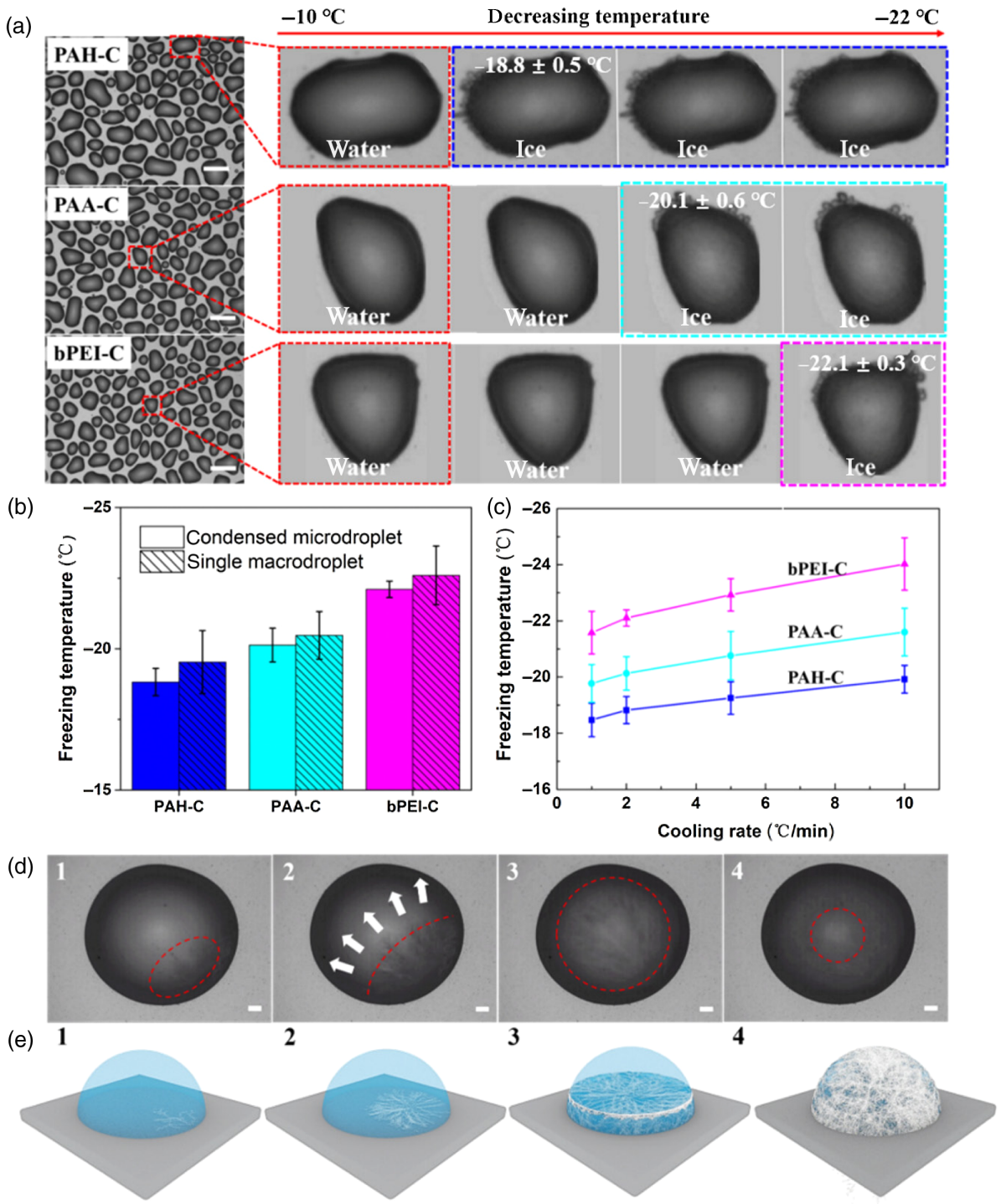

Figure 2 | *(a) Optical microscopy images of water microdroplets condensed onto the CP-modified silicon wafers. The red arrow indicates a drop in temperature from −10 to −22 °C. As the temperature decreases, the PAH-C coated surface freezes first, followed by PAA-C, and bPEI-C coated surfaces. Cooling rate: 2 °C min^{-1}; Scale bar: 100 μm. (b) Temperatures of ice nucleation of condensed microdroplets and single macrodroplets on the CP-modified surfaces. (c) Cooling rate dependence of ice nucleation temperature on CP-modified surfaces. (d) The freezing process of a water droplet on the bPEI-C-coated surface. Scale bar: 100 μm. (e) Illustration of the icing process on the bPEI-C coated surface. The error bars represent one standard deviation of uncertainty.*

Citation: *CCS Chem.* **2022**, Just Published. DOI: 10.31635/ccschem.022.202202087
Link to VoR: https://doi.org/10.31635/ccschem.022.202202087

to investigate the effect of solid surfaces on ice nucleation.[24,39,41,42]

Figure 2a shows the change of morphology and opacity of water microdroplets condensed onto the PAH-C (top), PAA-C (middle), and bPEI-C (bottom) modified surfaces with decreasing temperature. For temperatures down to –10 °C, water microdroplets remained in the liquid state on all CP-coated surfaces. As the temperature dropped below –19 °C, most of the water microdroplets on the PAH-C coated surface suddenly changed in opacity, and the edges of the microdroplets changed their shape, reflecting ice nucleation.[27] Although the ice nucleation is slower than the other stages in the icing process, the rapid growth results in the quasi-immediate freezing of water microdroplets upon the formation of ice nuclei.[43] Such ice nucleation does not occur until temperatures drop below –20 and –22 °C for microdroplets on the PAA-C and bPEI-C modified surfaces, respectively.

The average ice nucleation temperatures for condensed microdroplets and single macrodroplets are summarized in Figure 2b with a cooling rate of 2 °C min^{-1}. The freezing temperatures for condensed microdroplets on the PAH-C, PAA-C, and bPEI-C coated surfaces are –18.8 ± 0.5 °C, –20.1 ± 0.6 °C, and –22.1 ± 0.3 °C, respectively. Previously, Zhang et al.[44] immobilized short peptides onto surfaces as an anti-icing coating for the first time, and the freezing temperature was reduced to –16.3 °C, which is higher than that of the CP-coated surface in our study. Though supercharged polypeptides exhibited the same performance on tuning ice nucleation with the lowest freezing temperature of –22.8 ± 0.6 °C, easier synthesis and lower toxicity make the CPs more attractive for potential practical application, such as food storage and cryopreservation of cells and tissues.[27] To verify the data obtained with microdroplets, we also investigated the freezing of single macroscopic droplets on CP-coated surfaces, recording more than 200 independent freezing events. The ice nucleation temperature on CP-coated surfaces resembled a Gaussian distribution, as shown in Supporting Information Figure S7. In situ optical microscopic observation of macrodroplets showed a significant difference in freezing temperatures on the different CP-coated surfaces. The freezing temperatures of macrodroplets on the PAH-C, PAA-C, and bPEI-C coated surfaces displayed the same trend as that of the microdroplets. The average freezing temperature of macrodroplets was slightly lower than that of the condensed microdroplets, which can be rationalized by the presence of a temperature gradient when a cooling stage cools down macroscopic droplets.[27] Though the ice nucleation temperature decreased with increasing cooling rate, it showed the same trend of ice nucleation temperature for CP-coated surfaces with different cooling rates, that is, $T_{H,PAH\text{-}C} > T_{H,PAA\text{-}C} > T_{H,bPEI\text{-}C}$ (Figure 2c). When the cooling rate is too fast, the T_H would be affected due to the heat transfer effect,[45] providing a reasonable explanation for the observed cooling-rate dependence of the ice nucleation temperature, which agrees with previous reports.[46]

To investigate icing process on the CP-coated surfaces, a high-speed camera was employed to record the changes from water to ice on the bPEI-C coated surface. Then, we extracted sequential images of the bPEI-C modified surfaces before and after freezing. As shown in Figure 2d, the ice nucleation initiated at the liquid–solid interface, highlighted by the red circle. Then ice nuclei grew along the liquid–solid interface, followed by upward ice growth until the droplet was completely frozen, which is illustrated in Figure 2e. Different CP-coated surfaces lead to different HIN effects due to different interfacial interactions, which has been observed for microdroplets and single macrodroplets. It has been reported that ice nucleation is facilitated on a positively charged surface, while it is suppressed on a negatively charged surface.[41,47] This agrees with the result we obtained on positively charged PAH-C and negatively charged PAA-C. The ice nucleation temperature on the bPEI-C-coated surface was the lowest among the three CP-coated surfaces, although the PAH-C and bPEI-C have the same charge properties and functional groups. Further analysis showed that the effect of the CP chain length on ice nucleation was negligible (Supporting Information Figure S8).

A lower ice nucleation temperature implies a stronger interaction between the CP-coated surface and the water molecules, preventing the water molecules from organizing in an ice-like fashion.[46,48] In addition to electrostatic interactions, hydrogen-bonding interactions between water molecules and NH_2 or COOH groups in CPs may also play a role.[49] To test this hypothesis, the interfacial water structure at the CP/water interface was studied by measuring the $\mathrm{Im}\chi^{(2)}_{eff}$ spectra in the O–H stretch mode frequency region (3000–3600 cm^{-1}) using HD-SFG spectroscopy. The schematic illustration for HD-SFG measurement is shown in Figure 3a. The measured $\mathrm{Im}\chi^{(2)}_{eff}$ spectra for CPs in contact with 1 mM and 100 mM $NaClO_4$ solutions are shown in Figure 3b. The $\mathrm{Im}\chi^{(2)}_{eff}$ spectrum showed a positive band (3000–3500 cm^{-1}) for PAA-C, which was assigned to the stretching vibration of the hydrogen-bonded (H-bonded) O–H groups of water molecules.[50,51] The band was positive, indicating that the H-bonded O–H groups were oriented up to the PAA-C,[52] consistent with the fact that PAA-C is negatively charged. For both PAH-C and bPEI-C, H-bonded O–H bands were negative because they have a positively charged surface.

The difference between the $\mathrm{Im}\chi^{(2)}_{eff}$ spectra at the different ion concentrations (so-called $\chi^{(3)}$ contribution) reflects the charge of the interface.[53,54] The differential $\mathrm{Im}\chi^{(2)}_{eff}$ spectra ($\mathrm{Im}\Delta\chi^{(2)}_{eff}$ spectra) are displayed in Figure 3c. For PAA-C, the intensity of $\mathrm{Im}\Delta\chi^{(2)}_{eff}$ spectrum is very low, while for both PAH-C and bPEI-C, the $\mathrm{Im}\Delta\chi^{(2)}_{eff}$ spectral intensities are nearly zero. Such negligible

Citation: *CCS Chem.* **2022**, Just Published. DOI: 10.31635/ccschem.022.202202087
Link to VoR: https://doi.org/10.31635/ccschem.022.202202087

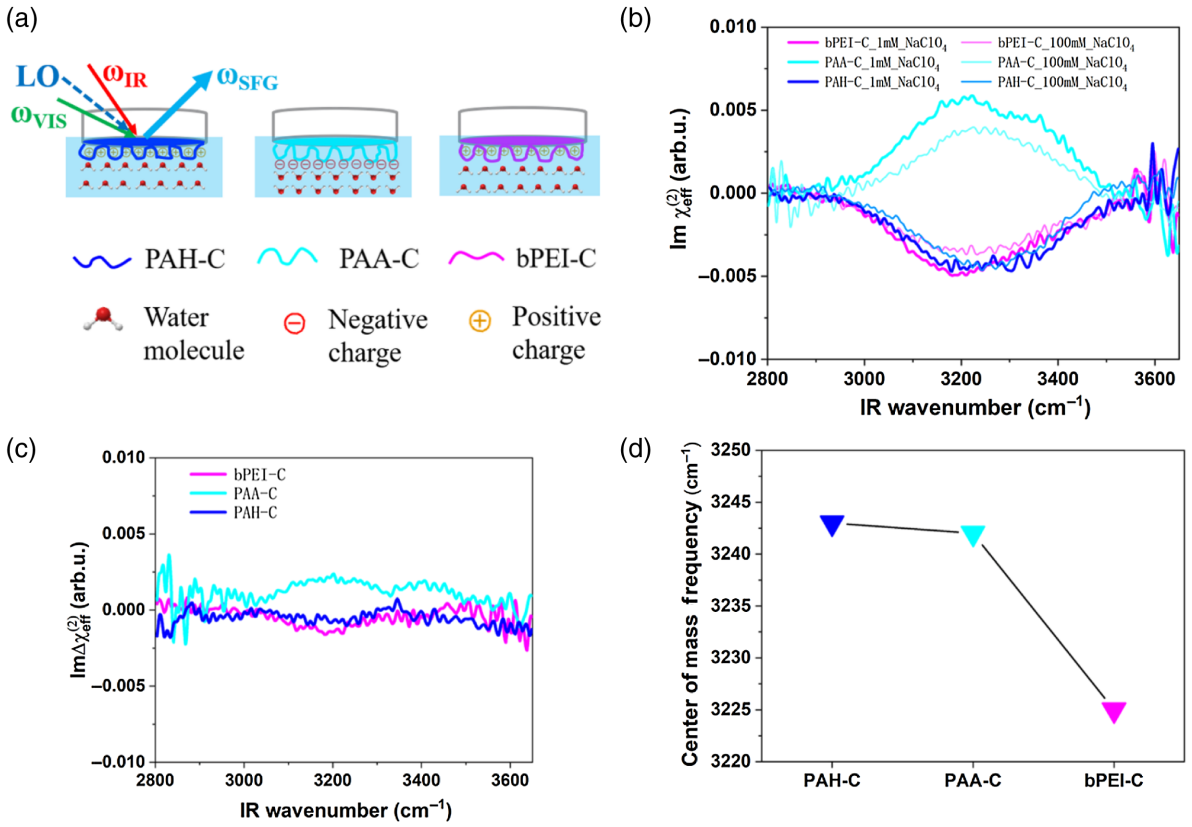

Figure 3 | *(a) Schematic illustration of the SFG measurements. PAH-C, PAA-C, and bPEI-C were coated on optical transparent silica substrates for SFG measurements. (b) Im $\chi^{(2)}$ spectra of water molecules at the CP/water interface for 1 mM and 100 mM $NaClO_4$ solution. (c) Differential Im $\chi^{(2)}$ spectra of water molecules at the CP/water interface for 1 mM and 100 mM $NaClO_4$ solution. (d) Center of mass frequency of H-bonded O–H band for CPs in contact with 100 mM $NaClO_4$ solution.*

difference means that the electrostatic interaction between CPs and water molecules is very weak possibly because ions may be intercalated into the CPs' network and then neutralize the CP surface (Figure 4a). In this case, the $\mathrm{Im}\chi^{(2)}_{\mathrm{eff}}$ spectra for different CPs are dominated by the contribution from the interfacial region.

By carefully inspecting the $\mathrm{Im}\chi^{(2)}_{\mathrm{eff}}$ spectra for different CPs measured at 100 mM, we found that the center-of-mass (COM) frequencies of the H-bonded O–H bands were different, as plotted in Figure 3b,d. The frequencies were 3243, 3242, and 3225 cm^{-1} for PAH-C, PAA-C, and bPEI-C coated surfaces, respectively. A higher COM frequency reflects weaker hydrogen bonding between water molecules and CPs, and vice versa.[55] For bPEI-C, the COM frequency was the lowest, implying the strongest hydrogen bonding strength, preventing water from rearranging to form crystalline ice-like structures when the sample is cooled down to lower temperatures. As such, the highest T_H for PAH-C coated surface correlates with the lowest extent of orientation of interfacial water and the weakest hydrogen bonding interaction. Thus, we propose that, for these relatively weakly charged surfaces, hydrogen bonding interactions rather than charge govern the ice nucleation for polyelectrolytes. The formation of ice was hindered by strong hydrogen bonding interaction and favored by weak hydrogen bonding interaction.

The ability of CPs to tune the ice nucleation was consolidated by measuring the delay time of ice nucleation (t_d), which was the duration taken from the starting time (the moment of maintaining a specific supercooling temperature) to the time of ice nucleation to occur. As shown in Figure 4a, the delay time was significantly different on the different CP-coated surfaces, for example, water froze on the PAH-C surface after ~50 s, whereas the water drop did not freeze until ~500 and ~1800 s on the PAA-C and bPEI-C surfaces, respectively. The trend of t_d of water droplets on different CP-coated surfaces shows the order of t_d (bPEI-C) > t_d (PAA-C) > t_d (PAH-C), which is consistent with the freezing temperature obtained from T_H (see Figure 2b), indicating agreement with the above experimental results.

To evaluate the stability of the bPEI-C coating, the silicon wafers fabricated by bPEI-C were kept in the

Citation: *CCS Chem.* **2022**, Just Published. DOI: 10.31635/ccschem.022.202202087
Link to VoR: https://doi.org/10.31635/ccschem.022.202202087

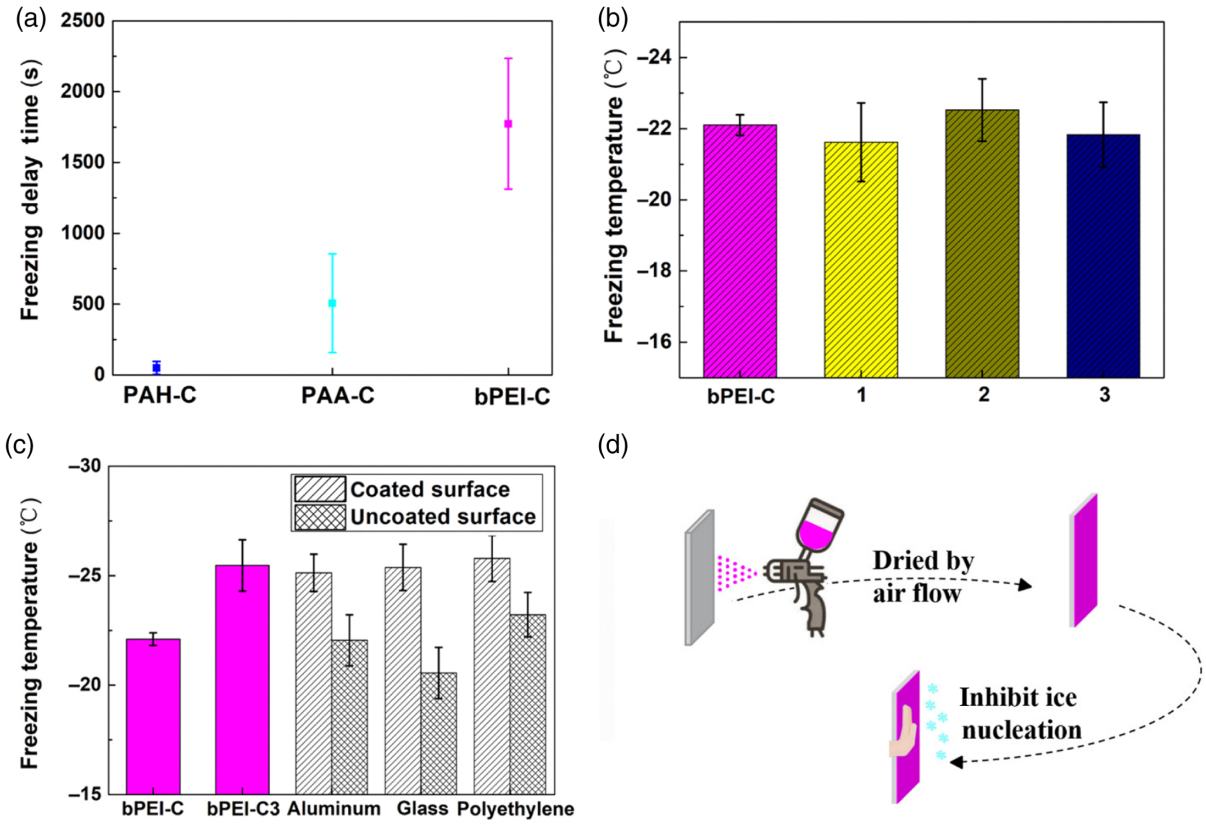

Figure 4 | *(a) Average delay times of ice nucleation measured at –18 °C on CP-coated surfaces. (b) The value of ice nucleation temperature on the bPEI-C coated surface before and after refrigeration (1), immersion in water (2), and immersion in 5 M NaCl solution (3) for up to 30 days. (c) Ice nucleation temperature on the bPEI-C coated silicon wafer, bPEI-C3 coated silicon wafer, and comparison of ice nucleation temperature before and after coating on aluminum, glass, and polyethylene with bPEI-C3. (d) Schematic representation of scale-up procedure for fabrication of CPs coating. The error bars represent one standard deviation of uncertainty.*

refrigerator, water, and NaCl solution with a concentration of 5 M for up to 30 days (Figure 4b). Then they were removed and rinsed with ultrapure water and dried with high purity nitrogen for measuring the ice nucleation temperature. We found the ice nucleation temperatures for the bPEI-C-coated surface after exposure to these harsh conditions indistinguishable from the newly prepared one, indicating excellent stability due to the strong adhesion of the bPEI-C coating, which was proved by Wang's group.[56]

To further enlarge the window of ice nucleation temperature, we increased the molar feed ratio between bPEI and DOPA from 10:1 to 10:3 (denoted as bPEI-C3), and then sodium periodate ($NaIO_4$) was added to induce the cross-linking (see Supporting Information Figure S9). Catechol was used as an anchoring group to deposit the bPEI onto different substrates and simultaneously as the site to cross-link the bPEI via $NaIO_4$-induced dismutation.[57] It has been proposed that there are two distinct states of water in the matrix of polyelectrolytes, that is, non-freezable water and freezable water, and the fraction of two types of water can be tailored via cross-linking the polyelectrolytes for tuning ice nucleation according to our previous work.[36] Thus, we studied the ice nucleation temperature of the bPEI-C3 coated surface and found that it was significantly decreased to a value of –25.5 °C. Moreover, to investigate the versatility of the CP coating, we compared the ice nucleation temperatures for three types of solid surfaces before and after coating with bPEI-C3, including aluminum, glass, and polyethylene, typical daily life materials. Figure 4c presents the differences between the coated surfaces and uncoated surfaces. For the coated surfaces, the ice nucleation temperatures were indistinguishable, indicating the ice nucleation temperature is independent of substrate. Moreover, lower ice nucleation temperature on the coated surface endows the coating a wider range of application.

Essentially, developing low-cost materials for regulating ice nucleation along with a facile and scalable procedure is critically important to promote the commercialization of

Citation: *CCS Chem.* **2022**, Just Published. DOI: 10.31635/ccschem.022.202202087
Link to VoR: https://doi.org/10.31635/ccschem.022.202202087

anti-ice-nucleation materials. In our case, the CPs are water-soluble and environmental-friendly, and they can adhere to virtually all types of substrates because of the strong adhesion of the catechol group. These advantages make it ideal for large-scale preparation. As a proof-of-concept, spraying is suitable for various solid substrates. Thus, we sprayed the glass with bPEI-C3 solution (Figure 4d), and the sprayed glass inhibited ice nucleation as thoroughly as the glass coated via the immersion method (Supporting Information Figure S10). We believe that developing such a scalable procedure for the preparation of anti-ice-nucleation material will be beneficial for its broad applications.

Conclusion

Inspired by mussel adhesive protein, three types of CPs have been synthesized by introducing catechol groups onto polyelectrolytes. We found that the bPEI-C-coated surface shows excellent performance in inhibiting ice nucleation. Our spectroscopic results indicate that hydrogen bonding interactions between the functional groups of the polyelectrolytes and the water molecules play a critical role in tuning ice nucleation. The bPEI-C coating exhibited excellent stability under harsh conditions and can be applied to various substrates via spray deposition for scalable production. Moreover, the window of ice nucleation temperature can be enlarged by inducing cross-linking. Thus, this comprehensive mechanic study provides molecular-level insights into how the polyelectrolytes affect the HIN and guidance for the rational design of anti-ice-nucleation materials in cryopreservation for organ transport and cell preservation.

Supporting Information

Supporting Information is available and includes experimental section, chemical structures, UV–vis spectra, FT-IR spectra, ^{1}H-NMR spectra, XPS spectra, AFM images, water contact angles, homebuilt experimental apparatus, distribution of ice nucleation temperatures of single macroscopic droplet, ice nucleation temperatures of CPs coated surfaces with different chain lengths, synthesis of bPEI-3 coating, and ice nucleation temperatures for different coating methods.

Conflict of Interest

There is no conflict of interest to report.

Funding Information

This research was financially supported by China Scholarship Council.

References

1. Janjua, Z.; Turnbull, B.; Hibberd, S.; Choi, K.-S. Mixed Ice Accretion on Aircraft Wings. *Phys. Fluids* **2018**, *30*, 027101.
2. Wang, Z.; Lin, B.; Sheng, S.; Tan, S.; Wang, P.; Tao, Y.; Liu, Z.; He, Z.; Wang, J. Bioinspired Anti-Icing Hydrogel Enabled by Ice-Nucleating Protein. *CCS Chem.* **2022**, *4*, 104–111.
3. Fakorede, O.; Feger, Z.; Ibrahim, H.; Ilinca, A.; Perron, J.; Masson, C. Ice Protection Systems for Wind Turbines in Cold Climate: Characteristics, Comparisons and Analysis. *Renew. Sust. Energ. Rev.* **2016**, *65*, 662–675.
4. Andersson, A. K.; Chapman, L. The Impact of Climate Change on Winter Road Maintenance and Traffic Accidents in West Midlands, UK. *Accid. Anal. Prev.* **2011**, *43*, 284–289.
5. Vercillo, V.; Tonnicchia, S.; Romano, J.; Garcia-Giron, A.; Aguilar-Morales, A.; Alamri, S.; Dimov, S.; Kunze, T.; Lasagni, A.; Bonaccurso, E. Design Rules for Laser-Treated Icephobic Metallic Surfaces for Aeronautic Applications. *Adv. Funct. Mater.* **2020**, *30*, 1910268.
6. Guo, Q.; He, Z.; Jin, Y.; Zhang, S.; Wu, S.; Bai, G.; Xue, H.; Liu, Z.; Jin, S.; Zhao, L.; Wang, J. Tuning Ice Nucleation and Propagation with Counterions on Multilayer Hydrogels. *Langmuir* **2018**, *34*, 11986–11991.
7. Moore, E.; Molinero, V. Structural Transformation in Supercooled Water Controls the Crystallization Rate of Ice. *Nature* **2011**, *479*, 506–508.
8. Chen, X.; Ma, R.; Zhou, H.; Zhou, X.; Che, L.; Yao, S.; Wang, Z. Activating the Microscale Edge Effect in a Hierarchical Surface for Frosting Suppression and Defrosting Promotion. *Sci. Rep.* **2013**, *3*, 2515.
9. Liu, Z.; Zheng, X.; Wang, J. Bioinspired Ice-Binding Materials for Tissue and Organ Cryopreservation. *J. Am. Chem. Soc.* **2022**, *144*, 5685–5701.
10. Liu, J.; Zhu, C.; Liu, K.; Jiang, Y.; Song, Y.; Francisco, J.; Zeng, X.; Wang, J. Distinct Ice Patterns on Solid Surfaces with Various Wettabilities. *Proc. Natl. Acad. Sci. U. S. A.* **2017**, *114*, 11285–11290.
11. Zhang, Z.; Liu, X.-Y. Control of Ice Nucleation: Freezing and Antifreeze Strategies. *Chem. Soc. Rev.* **2018**, *47*, 7116–7139.
12. Yang, S.; Wu, C.; Zhao, G.; Sun, J.; Yao, X.; Ma, X.; Wang, Z. Condensation Frosting and Passive Anti-Frosting. *Cell Rep. Phys. Sci.* **2021**, *2*, 100474.
13. Liu, J.; Guo, H.; Zhang, B.; Qiao, S.; Shao, M.; Zhang, X.; Feng, X.; Li, Q.; Song, Y.; Jiang, L.; Wang, J. Guided Self-Propelled Leaping of Droplets on a Micro-Anisotropic Superhydrophobic Surface. *Angew. Chem. Int. Ed.* **2016**, *55*, 4265–4269.
14. Jin, S.; Liu, J.; Lv, J.; Wu, S.; Wang, J. Interfacial Materials for Anti-Icing: Beyond Superhydrophobic Surfaces. *Chem. Asian J.* **2018**, *13*, 1406–1414.
15. Irajizad, P.; Hasnain, M.; Farokhnia, N.; Sajadi, S.; Ghasemi, H. Magnetic Slippery Extreme Icephobic Surfaces. *Nat. Commun.* **2016**, *7*, 13395.
16. Bengaluru Subramanyam, S.; Kondrashov, V.; Rühe, J.; Varanasi, K. Low Ice Adhesion on Nano-Textured

Citation: *CCS Chem.* **2022**, Just Published. DOI: 10.31635/ccschem.022.202202087
Link to VoR: https://doi.org/10.31635/ccschem.022.202202087

Superhydrophobic Surfaces under Supersaturated Conditions. *ACS Appl. Mater. Interfaces* **2016**, *8*, 12583–12587.
17. Ibáñez-Ibáñez, P.; Montes Ruiz-Cabello, F.; Cabrerizo-Vílchez, M.; Rodríguez-Valverde, M. Ice Adhesion of PDMS Surfaces with Balanced Elastic and Water-Repellent Properties. *J. Colloid Interface Sci.* **2022**, *608*, 792–799.
18. Wang, F.; Zhuo, Y.; He, Z.; Xiao, S.; He, J.; Zhang, Z. Dynamic Anti-Icing Surfaces (DAIS). *Adv. Sci.* **2021**, *8*, 2101163.
19. Kreder, M.; Alvarenga, J.; Kim, P.; Aizenberg, J. Design of Anti-Icing Surfaces: Smooth, Textured or Slippery? *Nat. Rev. Mater.* **2016**, *1*, 15003.
20. Lv, J.; Yao, X.; Zheng, Y.; Wang, J.; Jiang, L. Antiadhesion Organogel Materials: From Liquid to Solid. *Adv. Mater.* **2017**, *29*, 1703032.
21. Maitra, T.; Jung, S.; Giger, M.; Kandrical, V.; Ruesch, T.; Poulikakos, D. Superhydrophobicity vs. Ice Adhesion: The Quandary of Robust Icephobic Surface Design. *Adv. Mater. Interfaces* **2015**, *2*, 1500330.
22. Wang, Y.; Yao, X.; Chen, J.; He, Z.; Liu, J.; Li, Q.; Wang, J.; Jiang, L. Organogel as Durable Anti-Icing Coatings. *Sci. China Mater.* **2015**, *58*, 559–565.
23. Michaelides, A.; Morgenstern, K. Ice Nanoclusters at Hydrophobic Metal Surfaces. *Nat. Mater.* **2007**, *6*, 597–601.
24. He, Z.; Liu, K.; Wang, J. Bioinspired Materials for Controlling Ice Nucleation, Growth, and Recrystallization. *Acc. Chem. Res.* **2018**, *51*, 1082–1091.
25. Sun, Y.; Giubertoni, G.; Bakker, H.; Liu, J.; Wagner, M.; Ng, D.; Devries, A.; Meister, K. Disaccharide Residues Are Required for Native Antifreeze Glycoprotein Activity. *Biomacromolecules* **2021**, *22*, 2595–2603.
26. Voets, I.; Meister, K. Interaction of Antifreeze Proteins with Water. In *Antifreeze Proteins Volume 2: Biochemistry, Molecular Biology and Applications*; Ramløv, H., Friis, D. S., Eds.; Springer International Publishing: Cham, **2020**; pp 109–127.
27. Yang, H.; Ma, C.; Li, K.; Liu, K.; Loznik, M.; Teeuwen, R.; Van Hest, J. C. M.; Zhou, X.; Herrmann, A.; Wang, J. Tuning Ice Nucleation with Supercharged Polypeptides. *Adv. Mater.* **2016**, *28*, 5008–5012.
28. Xue, B.; Zhao, L.; Qin, X.; Qin, M.; Lai, J.; Huang, W.; Lei, H.; Wang, J.; Wang, W.; Li, Y.; Cao, Y. Bioinspired Ice Growth Inhibitors Based on Self-Assembling Peptides. *ACS Macro Lett.* **2019**, *8*, 1383–1390.
29. He, Z.; Zheng, L.; Liu, Z.; Jin, S.; Li, C.; Wang, J. Inhibition of Heterogeneous Ice Nucleation by Bioinspired Coatings of Polyampholytes. *ACS Appl. Mater. Interfaces* **2017**, *9*, 30092–30099.
30. Liu, Y.; Ai, K.; Lu, L. Polydopamine and Its Derivative Materials: Synthesis and Promising Applications in Energy, Environmental, and Biomedical Fields. *Chem. Rev.* **2014**, *114*, 5057–5115.
31. Lee, H.; Dellatore, S.; Miller, W.; Messersmith, P. Mussel-Inspired Surface Chemistry for Multifunctional Coatings. *Science* **2007**, *318*, 426–430.
32. Lee, H.; Lee, B.; Messersmith, P. A Reversible Wet/Dry Adhesive Inspired by Mussels and Geckos. *Nature* **2007**, *448*, 338–341.
33. Lee, B.; Messersmith, P.; Israelachvili, J.; Waite, J. Mussel-Inspired Adhesives and Coatings. *Annu. Rev. Mater. Res.* **2011**, *41*, 99.
34. Ahn, B.; Das, S.; Linstadt, R.; Kaufman, Y.; Martinez-Rodriguez, N.; Mirshafian, R.; Kesselman, E.; Talmon, Y.; Lipshutz, B.; Israelachvili, J.; Waite, J. High-Performance Mussel-Inspired Adhesives of Reduced Complexity. *Nat. Commun.* **2015**, *6*, 8663.
35. Hong, S.; Na, Y.; Choi, S.; Song, I.; Kim, W.; Lee, H. Non-Covalent Self-Assembly and Covalent Polymerization Co-Contribute to Polydopamine Formation. *Adv. Funct. Mater.* **2012**, *22*, 4711–4717.
36. Chen, J.; Li, K.; Wu, S.; Liu, J.; Liu, K.; Fan, Q. Durable Anti-Icing Coatings Based on Self-Sustainable Lubricating Layer. *ACS Omega* **2017**, *2*, 2047–2054.
37. Chen, J.; Luo, Z.; Fan, Q.; Lv, J.; Wang, J. Anti-Ice Coating Inspired by Ice Skating. *Small* **2014**, *10*, 4693–4699.
38. Guo, Z.; Mi, S.; Sun, W. A Facile Strategy for Preparing Tough, Self-Healing Double-Network Hyaluronic Acid Hydrogels Inspired by Mussel Cuticles. *Macromol. Mater. Eng.* **2019**, *304*, 1800715.
39. Huang, B.; Jiang, S.; Diao, Y.; Liu, X.; Liu, W.; Chen, J.; Yang, H. Hydrogels as Durable Anti-Icing Coatings Inhibit and Delay Ice Nucleation. *Molecules* **2020**, *25*, 3378.
40. Sedó, J.; Saiz-Poseu, J.; Busqué, F.; Ruiz-Molina, D. Catechol-Based Biomimetic Functional Materials. *Adv. Mater.* **2013**, *25*, 653–701.
41. Ehre, D.; Lavert, E.; Lahav, M.; Lubomirsky, I. Water Freezes Differently on Positively and Negatively Charged Surfaces of Pyroelectric Materials. *Science* **2010**, *327*, 672–675.
42. Jung, S.; Tiwari, M.; Poulikakos, D. Frost Halos from Supercooled Water Droplets. *Proc. Natl. Acad. Sci. U. S. A.* **2012**, *109*, 16073–16078.
43. Du, N.; Liu, X.; Hew, C. Ice Nucleation Inhibition: Mechanism of Antifreeze by Antifreeze Protein. *J. Biol. Chem.* **2003**, *278*, 36000–36004.
44. Zhang, Y.; Liu, K.; Li, K.; Gutowski, V.; Yin, Y.; Wang, J. Fabrication of Anti-Icing Surfaces by Short Alpha-Helical Peptides. *ACS Appl. Mater. Interfaces* **2018**, *10*, 1957–1962.
45. Wu, S.; He, Z.; Zang, J.; Jin, S.; Wang, Z.; Wang, J.; Yao, Y.; Wang, J. Heterogeneous Ice Nucleation Correlates with Bulk-like Interfacial Water. *Sci. Adv.* **2019**, *5*, eaat9825.
46. Jin, S.; Liu, Y.; Deiseroth, M.; Liu, J.; Backus, E.; Li, H.; Xue, H.; Zhao, L.; Zeng, X.; Bonn, M.; Wang, J. Use of Ion Exchange to Regulate the Heterogeneous Ice Nucleation Efficiency of Mica. *J. Am. Chem. Soc.* **2020**, *142*, 17956–17965.
47. Charpentier, T.; Neville, A.; Millner, P.; Hewson, R.; Morina, A. Development of Anti-Icing Materials by Chemical Tailoring of Hydrophobic Textured Metallic Surfaces. *J. Colloid Interface Sci.* **2013**, *394*, 539–544.
48. Liu, K.; Wang, C.; Ma, J.; Shi, G.; Yao, X.; Fang, H.; Song, Y.; Wang, J. Janus Effect of Antifreeze Proteins on Ice Nucleation. *Proc. Natl. Acad. Sci. USA* **2016**, *113*, 14739.
49. Ping, Z.; Nguyen, Q.; Chen, S.; Zhou, J.; Ding, Y. States of Water in Different Hydrophilic Polymers—DSC and FTIR Studies. *Polymer* **2001**, *42*, 8461–8467.

Citation: *CCS Chem.* **2022**, Just Published. DOI: 10.31635/ccschem.022.202202087
Link to VoR: https://doi.org/10.31635/ccschem.022.202202087

50. Bonn, M.; Nagata, Y.; Backus, E. Molecular Structure and Dynamics of Water at the Water-Air Interface Studied with Surface-Specific Vibrational Spectroscopy. *Angew. Chem. Int. Ed.* **2015**, *54*, 5560–5576.
51. Nihonyanagi, S.; Mondal, J.; Yamaguchi, S.; Tahara, T. Structure and Dynamics of Interfacial Water Studied by Heterodyne-Detected Vibrational Sum-Frequency Generation. *Annu. Rev. Phys. Chem.* **2013**, *64*, 579–603.
52. Yamaguchi, S.; Tahara, T. Heterodyne-Detected Electronic Sum Frequency Generation: "Up" Versus "Down" Alignment of Interfacial Molecules. *J. Chem. Phys.* **2008**, *129*, 101102.
53. Wen, Y.; Zha, S.; Liu, X.; Yang, S.; Guo, P.; Shi, G.; Fang, H.; Shen, Y.; Tian, C. Unveiling Microscopic Structures of Charged Water Interfaces by Surface-Specific Vibrational Spectroscopy. *Phys. Rev. Lett.* **2016**, *116*, 016101.
54. Seki, T.; Yu, X.; Zhang, P.; Yu, C.; Liu, K.; Gunkel, L.; Dong, R.; Nagata, Y.; Feng, X.; Bonn, M. Real-Time Study of On-Water Chemistry: Surfactant Monolayer-Assisted Growth of a Crystalline Quasi-2D Polymer. *Chem* **2021**, *7*, 2758–2770.
55. Morita, A.; Hynes, J. A Theoretical Analysis of the Sum Frequency Generation Spectrum of the Water Surface. *Chem. Phys.* **2000**, *258*, 371–390.
56. Zhang, C.; Xiang, L.; Zhang, J.; Liu, C.; Wang, Z.; Zeng, H.; Xu, Z. Revisiting the Adhesion Mechanism of Mussel-Inspired Chemistry. *Chem. Sci.* **2022**, *13*, 1698–1705.
57. Wu, J.; Zhang, L.; Wang, Y.; Long, Y.; Gao, H.; Zhang, X.; Zhao, N.; Cai, Y.; Xu, J. Mussel-Inspired Chemistry for Robust and Surface-Modifiable Multilayer Films. *Langmuir* **2011**, *27*, 13684–13691.

Citation: *CCS Chem.* **2022**, Just Published. DOI: 10.31635/ccschem.022.202202087
Link to VoR: https://doi.org/10.31635/ccschem.022.202202087